climate

Article

Hydrometeorological Conditions of the Volga Flow Generation into the Caspian Sea during the Last Glacial Maximum

Andrey Kalugin [1,*] and Polina Morozova [2]

[1] Water Problems Institute, Russian Academy of Sciences, 119333 Moscow, Russia
[2] Institute of Geography, Russian Academy of Sciences, 119017 Moscow, Russia
* Correspondence: andrey.kalugin@iwp.ru

Abstract: The goal of this study is to evaluate annual and seasonal inflow from the Volga catchment area to the Caspian Sea during the Last Glacial Maximum (LGM ~21,000 years ago) using paleoclimate modeling data. The first approach is based on the LGM simulation by the general circulation models (GCMs) in the framework of the Paleoclimate Modelling Intercomparison Project (PMIP4) and the Coupled Modelling Intercomparison Project (CMIP6). We used four GCMs: INM-CM4-8, MIROC-ES2L, AWI-ESM1-1-LR, and MPI-ESM1-2-LR. The second approach is based on the spatially distributed process-based runoff generation model using PMIP4-CMIP6 model data as boundary conditions. The use of the hydrological ECOMAG model allows us to refine estimates of the Volga runoff in comparison to GCM calculations by considering seasonal features of runoff generation related to periglacial vegetation distribution, permafrost, and streamflow transformation along the channel network. The LGM is characterized by a high uncertainty in meteorological values calculated for the Volga basin using various GCMs. The share of runoff from the three most flooded months from the annual calculated in the LGM was 95%, according to INM-CM4-8, while other GCMs ranged from 69–78%. Three GCMs (MIROC-ES2L, AWI-ESM1-1-LR, and MPI-ESM1-2-LR) showed 83–88% of the present-day value of precipitation in the Volga basin during cooling for more than 10 °C, while INM-CM4-8 showed a two-fold decrease. According to hydrological modeling results using data from three models, the annual Volga runoff was significantly higher than the present-day value, and, when using data from INM-CM4-8, it was lower.

Keywords: runoff generation; Volga River; Last Glacial Maximum; process-based hydrological modeling; PMIP4

Citation: Kalugin, A.; Morozova, P. Hydrometeorological Conditions of the Volga Flow Generation into the Caspian Sea during the Last Glacial Maximum. *Climate* **2023**, *11*, 36. https://doi.org/10.3390/cli11020036

Academic Editor: Elias Massoud

Received: 31 December 2022
Revised: 28 January 2023
Accepted: 31 January 2023
Published: 2 February 2023

1. Introduction

The Caspian Sea's level fluctuations could be more than 100 m during the last glacial period [1,2]. The Caspian Sea is a drainless lake, and its level is determined by the balance between the river runoff and net evaporation from its surface since the flow of the Volga River is about 80% of the total surface inflow to the Caspian Sea. Level fluctuations are highly dependent on the Volga flow. Using a hydrological model of flow generation from the Volga basin, it is possible to quantify inflow to the Caspian Sea to explain the reasons for the development of one or another transgressive or regressive stages of the sea level. For example, the maximum level estimates reconstructed by researchers using different paleogeographic methods for the Caspian Sea's best-known transgressive stages, such as the Early Khvalyn and Late Khvalyn (the level rise to about 50 m and 0 m a.s.l., respectively), are rather consistent with each other [3–6], but there is no consensus about dating and mechanisms of this events. Evaluation of the minimum sea level during regressive stages varies widely and is sometimes not defined. This is largely due to the much more complex conditions for determining such sea levels, as the sediments from that time are now submerged. On the other hand, in the Lower Volga region, there are many transects, from which the researchers can reconstruct the Caspian level during different cold and warm epochs of the Late Pleistocene and Holocene. The lowering of the Caspian Sea level during the Last Glacial Maximum (LGM) is one of the most difficult regressive stages to study. There is no complete consensus about the Caspian Sea level in the LGM. Quantitative estimates using paleogeographic methods are also not available [7,8]. Based on paleoclimatic modeling, the Caspian level was estimated to be 50 m lower than it is now [9]. However, this value appears to be overestimated because the authors correctly note that this approach does not consider the effect of increasing inflow into the northern part of the sea due to the spread of permafrost and the corresponding types of vegetation in the watershed. The sea level regression would be smaller if these factors were taken into account.

According to PMIP4-CMIP6 (the Paleoclimate Modelling Intercomparison Project (PMIP4), the Coupled Modelling Intercomparison Project (CMIP6) [10]), and INMIO-CICE oceanic model simulations, evaporation from the Caspian Sea decreased from 2% to 20% in the LGM compared to the preindustrial (PI, 1850 CE) experiment [11]. The Volga runoff was also reduced. The meltwater runoff from the Scandinavian Ice Sheet was not estimated. The difference in estimates between PMIP4-CMIP6 models ranges from 5% to 55% when compared to PI values. Such findings are insufficient to determine whether the Caspian's position during the LGM period was regressive or transgressive. Deep regression with a high degree of certainty can be ruled out. The volume of river runoff from the Caspian catchment area by the model that demonstrated the minimal values of Volga runoff in the LGM is sufficient to keep sea level from dropping below −45 m a.s.l. In this study, the Volga runoff of atmospheric genesis during the LGM was estimated. The contribution of additional meltwater from the Scandinavian Ice Sheet remains a debatable issue, as well as the ice sheet boundary [12]. Recent paleogeographic studies show that the contribution of glacial meltwater to the annual Volga runoff was mostly not significant during the LGM [13]. The hypothesis that the Upper Volga was underlain by a system of extensive glacial lakes was refuted [14] based on the results of luminescence dating and modeling of glacioisostatic deformations. Furthermore, based on paleogeographic studies, the factor of interbasin overflows during the study period was excluded, implying that the river basin configuration was approximated to the modern one.

Most of the studies based on modeling the Volga runoff use global hydrological models [15–18], in which hydrological cycle processes are described with simplifying assumptions and water regime estimates obtained contain considerable uncertainty because global hydrological models are not tested with observational data [19]. The Volga basin water-balance models were used to calculate a runoff at ten-day and monthly temporal resolutions [20,21]. More reliable estimates of changes in the water regime caused by climate change can be obtained via process-based models of the hydrological cycle with distributed parameters [22,23]. Most of the parameters of such models are set from the global land surface databases.

In this study, we used the detailed process-based runoff generation model [24], which allows efficient calculation of daily river flow in different parts of the Volga basin simultaneously. Such models take into account regional features of river flow formation related to the distribution of various types of vegetation and permafrost, as well as snow accumulation and snowmelt processes on watershed and streamflow transformation along the channel network. These models enable researchers to investigate the physical mechanisms of flow formation, including different components of the hydrological cycle and the sensitivity of hydrological systems to climate change. These aspects should be considered when modeling the runoff formation in such contrasting climatic conditions as the LGM. This reduces the uncertainty associated with calculating the water regime under fundamentally different climatic conditions than those under which hydrological models have been validated [25]. The goal of this study is to estimate the annual and seasonal runoff of the Volga River during the LGM using paleoclimate modeling data. The first approach is based on the LGM simulation by PMIP4-CMIP6. The second approach is based on the spatially distributed process-based runoff generation model using PMIP4-CMIP6 model data as boundary conditions. For the first time, quantitative estimates of flow generation from the Volga basin to the Caspian Sea were obtained using a detailed hydrological model for the LGM.

2. Object, Data, and Methods

2.1. Study Basin

The Volga River is the largest river in Europe in terms of the basin area (1,360,000 km^2) and river length (3530 km). The Volga River basin is located between 48° to 62° N and 32° to 60° E (Figure 1). The natural water regime is characterized by spring floods, summer and winter low-water periods, and autumn rain floods. Spring floods occur in various parts of the Volga basin from April to June. The source of the Volga is 228 m a.s.l., and the river mouth in the Caspian Sea is −28 m a.s.l. The structure of the landscapes, by area of distribution, is dominated by grass crops, cool mixed forests, evergreen forests and fields, and narrow conifers. Table 1 presents the hydrometeorological characteristics of the Volga basin according to our estimates using station data for the period 1985–2014 (http://meteo.ru/english/climate/cl_data.php, accessed on 31 December 2022).

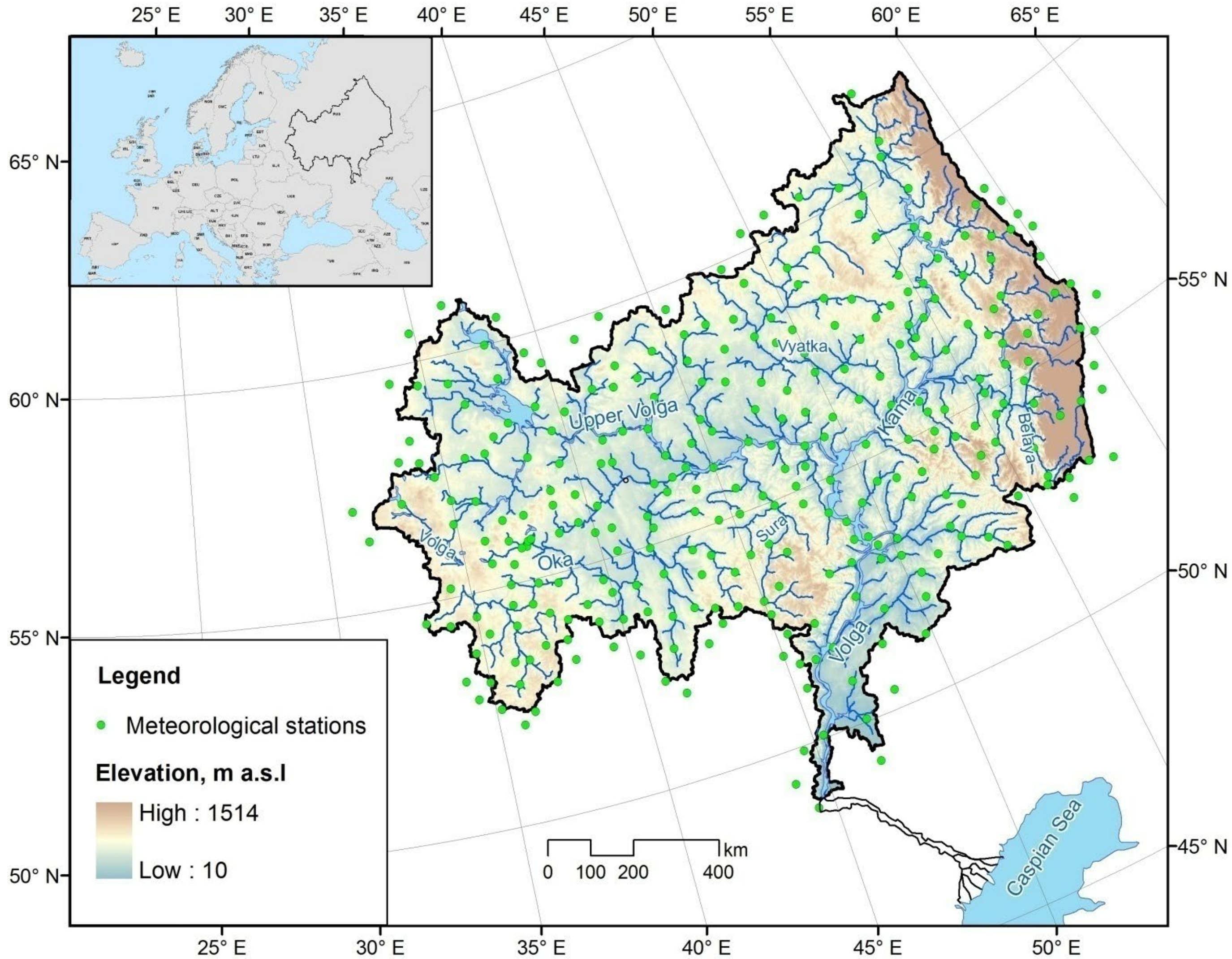

Figure 1. The Volga River basin and meteorological stations, whose data were used to calculate runoff using the hydrological model.

Table 1. Hydrometeorological characteristics of the Volga basin according to our estimates using data for the period 1985–2014.

Characteristic	Value
Mean annual air temperature	4 °C
Mean winter air temperature	−8 °C
Mean spring air temperature	8 °C
Mean summer–autumn air temperature	13 °C
Duration of the period with negative air temperature	Novermber-March
Annual precipitation	585 mm
Solid precipitation	30% of the annual total
Liquid precipitation	70% of the annual total
Annual runoff	260 km^3
Winter runoff	23%
Spring flood runoff	53%
Summer–autumn runoff	24%
Runoff coefficient	0.37

2.2. PMIP4-CMIP6 Model Data

The PMIP4-CMIP6 LGM model outputs are used here. The LGM was the last period when global ice volume was at a maximum, with ice sheets covering Fenoscandia and North America. Because the sea level was lower (about 115–130 m below the present sea level), it caused changes in coastlines and bathymetry. Greenhouse gas concentration was lower than the present, and astronomical parameters were also different. All these features are included in boundary conditions for the PMIP4-CMIP6 LGM experiment, which is described in detail in [26]. More information about models, simulations, and preliminary results are in [27]. For the LGM experiment (Table 2), we used all model data available on the website CMIP6 (https://esgf-node.llnl.gov/search/cmip6/, accessed on 31 December 2022) for most of 2022. New data for another model (CESM2) are also now available, but we did not use it in this study. All models used the same ICE 6G_C ice sheet reconstruction [28]. The Volga catchment area includes 67 cells of INM-CM4-8, 25 cells of MIROC-ES2L, 58 cells of AWI-ESM1-1-LR and MPI-ESM1-2-LR. Model data were averaged for the entire basin. The last 100 years of simulations have been analyzed.

Table 2. PMIP4-CMIP6 models used in this study.

Model Name, Reference	Resolution, Number of Cells (Longitude × Latitude)	Dynamic Vegetation
AWI-ESM-1-1-LR [29]	192 × 96	yes
INM-CM4-8 [30]	180 × 120	no
MIROC-ES2L [31]	128 × 64	no
MPI-ESM1-2-LR [32]	192 × 96	no

2.3. Hydrological Model

In the second approach, the Volga runoff was calculated based on the hydrological model with distributed parameters, which was developed on the platform of the ECOMAG (ECOlogical Model for Applied Geophysics) software [33]. The PMIP4-CMIP6 LGM experiment model data were used as boundary conditions in the runoff generation model. ECOMAG is focused on reproducing the processes of the hydrological cycle and allows calculating the spatial distribution of the snow cover and the snowmelt formation, soil freezing and thawing, vertical heat and moisture transport in frozen and unfrozen soil, evapotranspiration, surface, subsurface and groundwater flow, and streamflow transformation in the channel system. The ECOMAG model has been used successfully for more than ten years to describe hydrological processes and river water regimes in watersheds ranging from a few square kilometers to millions of square kilometers across North America and Eurasia [34–41].

Modeling of hydrological processes at each hydrological response unit (HRU) is performed for four levels: the topsoil layer, horizon of caliche, groundwater, and prechannel flow. During the cold season, snow cover is added. In the model, the subsurface and groundwater flow is described according to the Darcy equation, and the prechannel and stream flow is described by the kinematic wave equation. The total porosity in the soil aeration zone is divided into the capillary and non-capillary zones. Potential evaporation is estimated according to the Dalton method. The snowmelt rate is calculated using the degree-day method. The phase transformation of precipitation depends on the air temperature. The evaporation of solid and liquid phases of snow is estimated using data on the air humidity deficit. Infiltration of rain and meltwater into frozen soil is calculated considering the effect of ice content in frozen soil on the hydraulic conductivity of the soil. A more detailed mathematical description of the flow generation processes in the ECOMAG model is presented in [42]. Basin schematization requires a digital elevation model (any detail depending on catchment size and study objectives) and raster data on soil types and landcover types. The input data for the model are the daily air temperature, humidity deficit, and precipitation, which can be set either on a regular grid (General Circulation Models (GCMs)) or on an irregular grid (meteorological stations).

In the Volga basin model, HYDRO1k digital elevation model, Harmonized World Soil, and Global Landcover databases were used to schematize the watershed and determine land surface parameters. Each of the 775 HRUs with an average area of 1760 km^2 has its own set of soil and landcover types and topography. At the stage of model verification in present-day climate, the long-term series of daily air temperature, humidity, and precipitation, measured at 306 meteorological stations, were set as boundary conditions. Due to the availability of the Volga–Kama reservoir cascade, a spatial assessment of hydrological modeling quality was conducted simultaneously for a set of river gauges on the eight largest unregulated tributaries of the Volga with the catchment areas ranging from 18,500 to 244,000 km^2 [24]. Model parameters were calibrated for the period of 2000–2014 and verified for the period of 1986–1999 for the same gauges. The following numerical experiment was carried out to assess the accuracy of the Volga runoff calculation at the outlet gauge. As model boundary conditions in eight gauges (river runoff which makes up 3/4 of the Volga runoff), the observed daily discharge was set, and from the rest part of the basin, the runoff was calculated using meteorological station data with the same model parameters that were determined for the period of its calibration. Thus, the calculated daily flow of the Volga in natural conditions was obtained over a multi-year period. The averaged-basin (set of gauges) Nash-Sutcliffe criterion for daily flow and a relative systematic error of PBIAS calculation were 0.82 and 6% for the period of the model-parameter calibration, respectively, and 0.80 and 7% for the period of verification.

2.4. Hydrological Modeling Using the PMIP4-CMIP6 Data

We used monthly PMIP4-CMIP6 data for hydroclimatic calculations in the LGM. At the output, the monthly averaged-basin air temperature, humidity deficit, precipitation, and runoff depth were analyzed. The period 1985–2014 was chosen as a baseline for comparison using meteorological station data. Paleoclimatic norms of monthly meteorological values calculated by GCMs were transformed into series of corresponding daily values using the delta-change method (see, e.g., [43]). For the transformation, daily data from meteorological observations at 306 meteorological stations in the Volga basin for the modern period were used. A constant multiplier for precipitation and air humidity, as well as a constant value for air temperature, were applied to the daily precipitation, air temperature, and humidity measured at 306 meteorological stations. The transformation resulted in a series of daily data where the norms of mean monthly values in the transformed series became equal to the paleoclimatic averaged-basin norms in the LGM for each of the four GCMs. The series of daily meteorological values were set as boundary conditions in the hydrological model. Anomalies of the Volga flow in the LGM were determined relative to the norm of the natural flow (without taking into account the influence of the Volga–Kama reservoir cascade) corresponding to the current climate for the period of 1985–2014 based on the calculation results.

Permafrost spreading in the Volga paleocatchment may have influenced the generation of inflow to the Caspian Sea during the LGM. Based on the information about the climatic limits of permafrost spreading at the isotherm of mean annual air temperature below −5 °C [44], their spreading was taken into account in hydrological model calculations with paleoclimatic data on a 10 °C decrease in mean annual air temperature in the Volga basin relative to the present-day climate. Depending on the meteorological data for one or another GCM, the hydrological model accounted for permafrost distribution by freezing the initial conditions and annual formation of the seasonally thawed layer during the warm season. According to [45], almost the entire Volga basin was perennially frozen during the LGM. In addition to paleoclimatic data and the possible distribution of permafrost in the Volga basin, the hydrological model took into account the transformation of the vegetation cover based on the paleogeographic generalizations [45]. During the LGM, periglacial tundra was common in the Upper Volga and almost the entire Oka basin, and periglacial steppe and forest–steppe were common in the rest of the Volga basin. Thus, the numerical experiments with the hydrological model to calculate the Volga flow during the LGM included a combination of paleoclimatic data from each of the four GCMs and the land surface parameters expressed in the permafrost distribution and the corresponding vegetation types in the watershed.

3. Results

3.1. Runoff Calculations Using the PMIP4-CMIP6 Data

The PMIP4-CMIP6 LGM experiment data were compared to Volga basin station data (Table 3). According to GCMs, the winter period DJF was colder by 15–25 °C, the summer period JJA was colder by 4–6 °C, and the spring MAM and autumn SON were colder by 9–16 °C (Figure 2). The period with a negative temperature in the LGM lasted from October to April. The average annual temperature in the central part of the East European Plain west of the Volga basin was about −6 °C [46]. According to paleobotanical data reconstruction, the coldest month's temperature was about −14 ÷ −13 °C lower than the modern values, and the warmest month's temperature was about −9 ÷ −7 °C lower. The annual precipitation sum was lower by all the GCM data, but the precipitation sum simulated by INM-CM4-8 was 1.7–1.8 lower than the precipitation sum simulated by the other models. When compared to the PI experiment, the LGM decreased by 18% for AWI-ESM1-1-LR, 50% for INM-CM4-8, 29% for MIROC-ES2L, and 36% for MPI-ESM1-2-LR [11].

Table 3. The meteorological output of GCMs in the LGM was compared to station data (1985–2014).

Characteristics	AWI-ESM1-1-LR	INM-CM4-8	MIROC-ES2L	MPI-ESM1-2-LR
Average annual air temperature	−9.9 °C	−15.5 °C	−12.1 °C	−12 °C
December–February	−14.4 °C	−25 °C	−19.6 °C	−16.3 °C
March–May	−12.1 °C	−16.3 °C	−13.1 °C	−13.4 °C
June–August	−4.2 °C	−4.8 °C	−4 °C	−6.6 °C
September–November	−9 °C	−16 °C	−11.8 °C	−11.7 °C
Period with negative temperature	−13.1 °C	−21.6 °C	−16.9 °C	−15.0 °C
Warm period	−5.4 °C	−7.1 °C	−5.5 °C	−7.8 °C
Annual precipitation	−12.2%	−51%	−17%	−12.5%
Solid precipitation	49%	−6%	19%	35%
Liquid precipitation	−42%	−73%	−34%	−35%

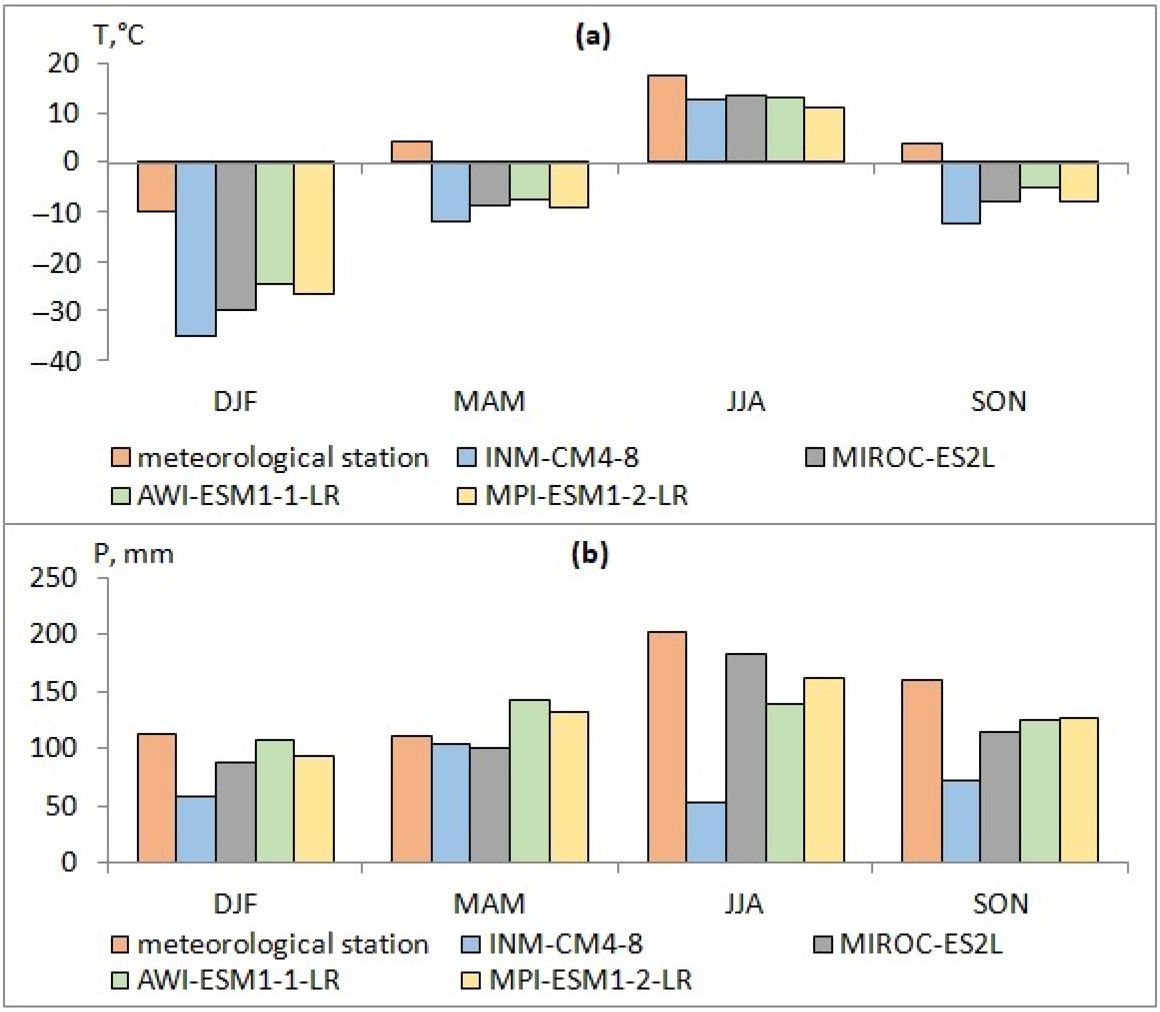

Figure 2. Seasonal averaged-basin values of air temperature (**a**) and precipitation (**b**) in the Volga basin for the LGM, according to the PMIP4-CMIP6 data, and present-day climate, according to meteorological stations.

The Volga runoff anomalies obtained by GCMs in the LGM were compared to simulated runoff by hydrological model for the modern period based on meteorological stations. The annual runoff depth during the LGM was 77 mm according to INM-CM4-8, or about one-third of modern value, two third according to MIROC-ES2L, and about half according to AWI-ESM1-1-LR and MPI-ESM1-2-LR. The winter runoff from November to March was 4%, according to INM-CM4-8, 13%, according to MIROC-ES2L, and about 50%, according to AWI-ESM1-1-LR and MPI-ESM1-2-LR; spring flood was 62%, according to INM-CM4-8, 89%, according to MIROC-ES2L, and 45–47%, according to AWI-ESM1-1-LR and MPI-ESM1-2-LR; the summer–autumn runoff was 5%, according to INM-CM4-8, and 58–62%, according to other GCMs (Figure 3). Note that the three most flooded months in this case for all GCMs in the LGM and in the present-day climate were April–June, although with significantly different proportions of the runoff relative to the annual runoff, which, when calculated from meteorological station data, was 54% of annual value, according to INM-CM4-8 it was 94%, MIROC-ES2L—75%, and according to AWI-ESM1-1-LR and MPI-ESM1-2-LR it was 50%. Summer–autumn runoff is significantly higher according to three GCMs than using INM-CM4-8. During the flood period, MIROC-ES2L indicates 1.4 times more runoff than INM-CM4-8, while AWI-ESM1-1-LR and MPI-ESM1-2-LR indicate 1.3–1.4 times less. Annual runoff for the three GCMs was 1.4–1.8 times higher than according to INM-CM4-8.

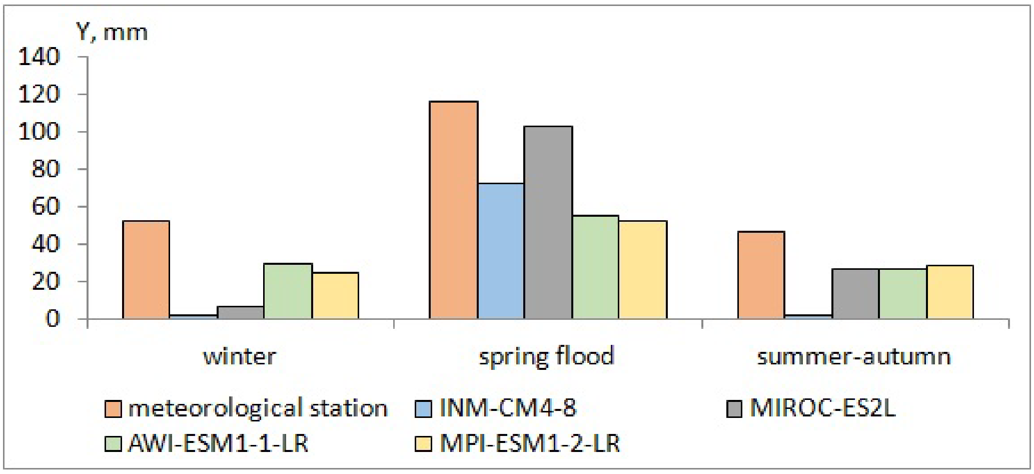

Figure 3. Seasonal runoff depth of the Volga River in the LGM calculated from the PMIP4-CMIP6 data and simulated by the hydrological model for the modern period based on meteorological stations.

However, due to the simplified parameterization of the flow formation processes and the sparse calculation grid, GCMs reproduce it with a large error, particularly the dynamics of the seasonally thawed layer under permafrost in the LGM, as well as the vegetation types typical for that time, and finally, a streamflow transformation along the channel network of such a large river basin. All of these factors have a significant impact on the generation of seasonal runoff. As a result, an attempt was made to specify the magnitude of the Volga runoff during the LGM using a detailed hydrological model based on the ECOMAG, which has greater spatial and temporal details than GCMs.

3.2. Runoff Calculations Based on Hydrological Model Using the PMIP4-CMIP6 Data

The annual and seasonal runoff calculated from the hydrological model using GCM data on boundary conditions was generally higher than the runoff estimated from the GCMs. In annual terms, the increase was 1.6 times for INM-CM4-8, 2.1 times for MIROC-ES2L, 2.7 times for AWI-ESM1-1-LR, and 3.5 times for MPI-ESM1-2-LR. The runoff increase calculated by the hydrological model during the flood period was 1.6 times higher by INM-CM4-8, 1.9 times higher by MIROC-ES2L, 4.2 times higher by AWI-ESM1-1-LR, and 4.9 times higher by MPI-ESM1-2-LR. This is due to the runoff formation model taking into account the distribution of the permafrost and the types of periglacial vegetation, which contribute to an increase in the runoff coefficient.

The use of a hydrological model allows for a more accurate consideration of the spring flood period due to the streamflow transformation along the channel network to the outlet gauge. If the high water was observed from April to June, according to GCM data, then using this data and the runoff formation model, the meltwater wave shifts on average one month later from May to July. Accordingly, the winter low-flow period was six months long from November to April, and summer–autumn runoff period was estimated to be three months long from August to October. At the same time, the share of seasonal runoff in the Volga relative to annual runoff changed insignificantly according to INM-CM4-8 and MIROC-ES2L data in comparison to the PMIP4-CMIP6 runoff data. The difference is less than 4%. According to AWI-ESM1-1-LR and MPI-ESM1-2-LR data, the share of runoff during the spring flood period increased by 28% and 19%, respectively, while the share of runoff during summer–autumn and winter periods decreased by 5% and 18%, respectively.

According to INM-CM4-8, the Volga runoff was 41% lower than calculated for present-day climate but higher, according to data from other GCMs, by 31, 40, and 74%, respectively. According to INM-CM4-8, runoff increased by 2% during the spring flood period but decreased by more than 90% during the rest of the year (Figure 4). According to MIROC-ES2L, spring flood runoff was 1.7 times higher, summer–autumn runoff was 7% higher, and winter runoff was 53% lower. According to AWI-ESM1-1-LR, spring flood runoff was twice as high, while summer–autumn and winter runoff volumes were 16% and 59% lower, respectively. According to MPI-ESM1-2-LR, spring flood runoff was 2.2 times higher, summer–autumn runoff was 1.5 times higher, and winter runoff was 27% lower.

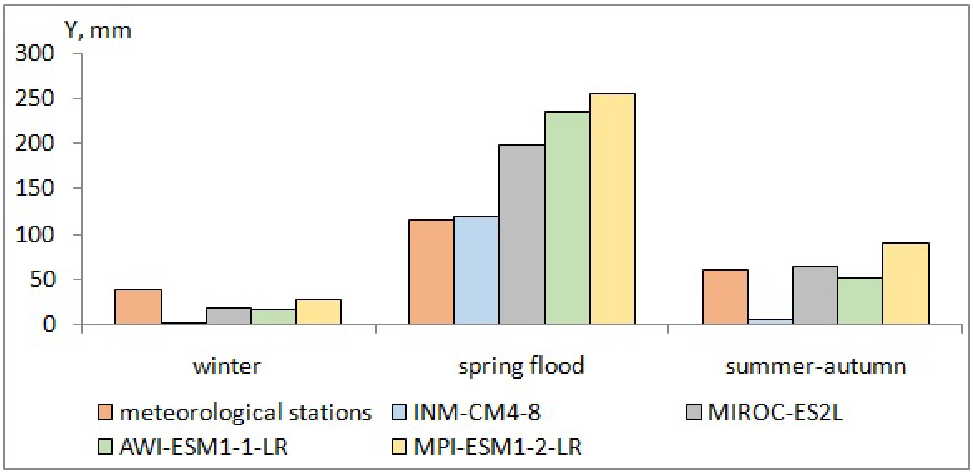

Figure 4. Seasonal runoff depth of the Volga River calculated by the runoff generation model using the PMIP4-CMIP6 data for the LGM and meteorological station data for the modern period.

The natural runoff during the three most flooded months from April to June was 54% of the annual value under present-day climate conditions. According to INM-CM4-8, the share of runoff from the three most flooded months from the annual calculated in the LGM was 95%, while other GCMs ranged from 69–78% (Figure 4). Summer–autumn runoff calculated by MIROC-ES2L, AWI-ESM1-1-LR, and MPI-ESM1-2-LR was 16–24% greater than that calculated by INM-CM4-8.

The detailed hydrological model allows for the estimation of the daily runoff changes. Thus, we calculated the change in the maximum water discharge in the Volga at the outlet gauge based on various GCMs. Peak annual discharge during the spring flood was 2 times higher, or about 67,000 $m^3\ s^{-1}$, according to INM-CM4-8, 2.1 times higher or 69,900 $m^3\ s^{-1}$, according to MIROC-ES2L, 2.5 times higher or 83,600 $m^3\ s^{-1}$, according to AWI-ESM1-1-LR, and 2.8 times higher or 94,000 $m^3\ s^{-1}$, according to MPI-ESM1-2-LR, due to the increased snow accumulation during the long cold period (Figure 5).

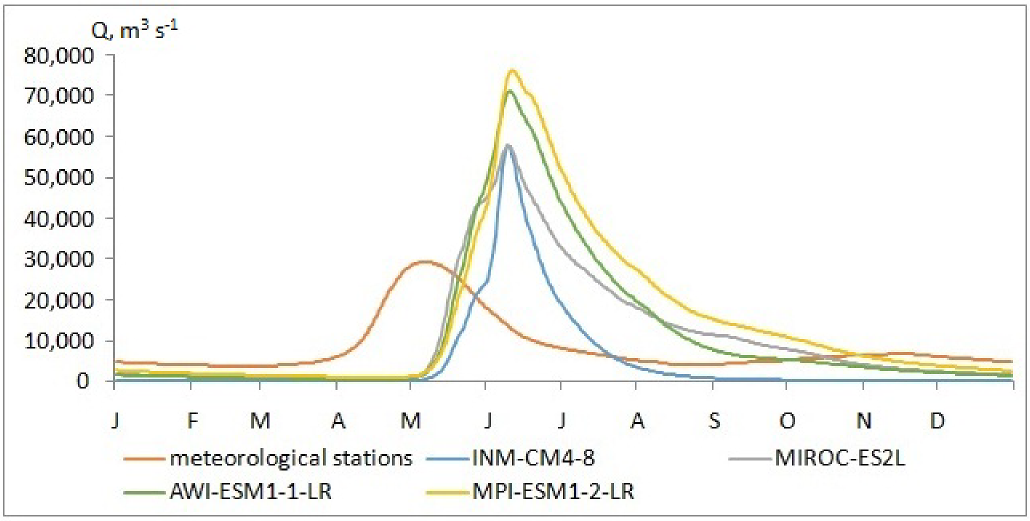

Figure 5. Mean multiyear daily discharge of the Volga River at the outlet gauge calculated by the runoff generation model using the PMIP4-CMIP6 data for the LGM and meteorological station data for the modern period.

4. Discussion

High snow water equivalent is one of the causes of the increased Volga runoff during a spring flood and peak annual discharge in the LGM epoch. According to the hydrological simulation results using INM-CM4-8 data, the maximum-averaged basin snow water equivalent increased by 29% compared to the simulation using observations, reaching 56% for MIROC-ES2L, 91% for AWI-ESM1-1-LR, and 84% for MPI-ESM1-2-LR (Figure 6). In the LGM, the maximum snow water equivalent was formed in early May, which was 1.5 months later than the value corresponding to the present-day climate. Only July and August were free of snow in the Volga basin.

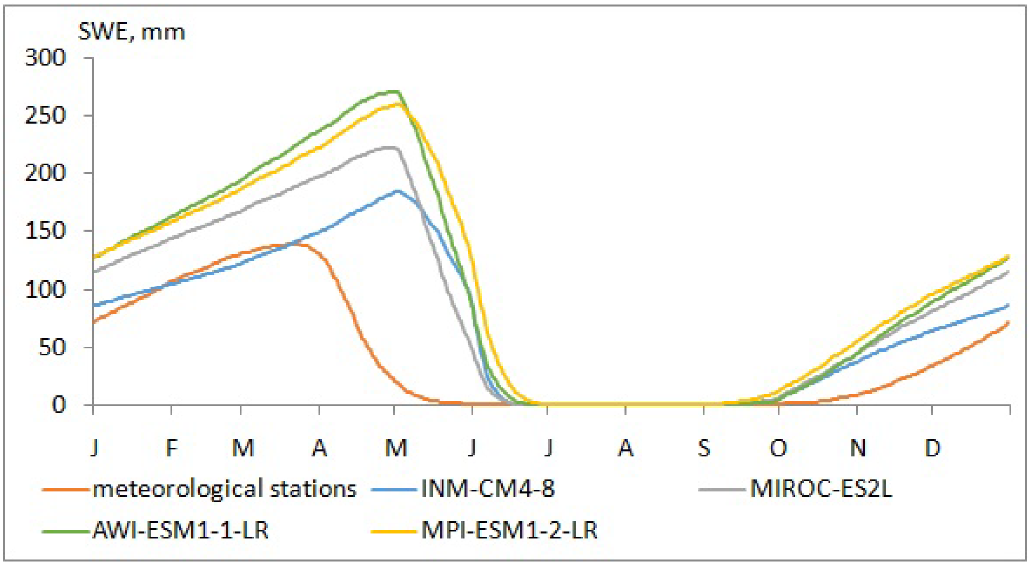

Figure 6. Snow water equivalent based on hydrological model calculations using the PMIP4-CMIP6 data for the LGM and meteorological station data (1985–2014).

Furthermore, the presence of periglacial vegetation causes less flattening of flood waves, resulting in a more intense increase in runoff during snow melting and an increase in peak discharge. In the LGM, the share of solid precipitation in the annual total increases by 1.4–1.9 times, and the duration of the cold season increases by more than two months, resulting in prolonged snowmelt and decreasing water losses for infiltration and evaporation of soil moisture against the background of permafrost spreading. As a result, the Volga runoff coefficient rises from 0.37 to 0.44 for INM-CM4-8, 0.58 for MIROC-ES2L and AWI-ESM1-1-LR, and 0.73 for MPI-ESM1-2-LR. Earlier work [47] demonstrated that the effect of continuous freezing of soils without thawing during the warm season in the Volga basin, using this runoff generation model for present-day climate conditions, leads to an 85% increase in the annual Volga runoff up to 460 km^3. The hydrological simulations for LGM conditions included the formation of a seasonally thawed layer during the summer period. In the calculations based on the INM-CM4-8 data, the average depth of the seasonally thawed layer in the Volga basin was 13 cm, on the MIROC-ES2L—27 cm, on the AWI-ESM1-1-LR—29 cm, and on the MPI-ESM1-2-LR—35 cm.

Although the precipitation over the Volga basin was overestimated by GCMs [48], the runoff depth determined by the water-balance method was low. This fact reduces the level of confidence in runoff depth values calculated by GCMs, at least in mid to high-latitude river basins with predominant snowmelt runoff and possible permafrost spread during the LGM epoch. The LGM is distinguished by a high uncertainty in meteorological values calculated by various GCMs for the Volga basin. The mean annual air temperature was estimated to be 5.5 °C. At the same time, the spread of reproduction for the cold period of the year was greater than for the warm period—8.5 °C and 2.5 °C, respectively. The decrease in precipitation is much smaller in MIROC-ES2L, AWI-ESM1-1-LR, and MPI-ESM1-2-LR with a 10–12 °C cooling in the LGM than in INM-CM4-8. According to MIROC-ES2L, the annual precipitation in the Volga basin was 488 mm; for AWI-ESM1-1-LR, it was 515 mm, and for MPI-ESM1-2-LR, it was 513 mm, corresponding to 83–88% of the present-day value. In comparison, the precipitation of 287 mm calculated by INM-CM4-8 was twice as low. According to the palaeobotanical reconstruction methodology [46], the decrease in precipitation during the LGM calculated by MIROC-ES2L, AWI-ESM1-1-LR, and MPI-ESM1-2-LR is close to the minimum estimate. On the contrary, the decrease by INM-CM4-8 is too strong and is close to the maximum estimate.

5. Conclusions

The annual river flow calculated from the hydrological model using GCMs data on boundary conditions was 1.6 times higher than the flow estimated in the GCMs themselves by INM-CM4-8, 2.1 times by MIROC-ES2L, 2.7 times by AWI-ESM1-1-LR, and 3.5 times by MPI-ESM1-2-LR. The annual runoff of the Volga River in the LGM calculated by the hydrological model was 151 km^3 for INM-CM4-8, 341 km^3 for MIROC-ES2L, 364 km^3 for AWI-ESM1-1-LR, and 453 km^3 for MPI-ESM1-2-LR. During the LGM, the snowmelt floods accounted for 70–95% of annual runoff. The MPI-ESM1-2-LR runoff is higher due to a lower air humidity deficit, e.g., by 32% compared to AWI-ESM1-1-LR, which contributes to less precipitation loss due to soil moisture evaporation. In other words, according to the runoff generation modeling using MIROC-ES2L, AWI-ESM1-1-LR, and MPI-ESM1-2-LR data, the Volga runoff increase in the LGM was large enough to form the maximum stage of the Caspian Sea's Khvalyn transgression, which modern paleogeographers refer to as the deglaciation period after the LGM [2,6,49]. Conditions for the Caspian Sea regression were potentially in the LGM, according to the flow generation modeling using INM-CM4-8 data, but not more than −45 m a.s.l [11]. The uncertainty of the Caspian Sea level change is associated with additional water input sources, such as the contribution of the glacial meltwater to Volga runoff or changes in the catchment of the Caspian Sea; however, it is beyond the scope of this study.

Based on the findings, it is suggested that the process-based hydrological models, previously validated for the subject of study of the observation period, are to be used to calculate river runoff using GCMs data from contrasting climatic epochs, such as the LGM. Such models enable detailed consideration of the land surface changes associated with vegetation transformation and permafrost formation. It is especially important to quantify river inflow into the Caspian Sea during different Late Pleistocene and Holocene periods to explain some physical causes of transgressive and regressive sea-level stages. Another direction to improve the Volga flow evaluation is to account for the melt component caused by the ice sheet degradation.

Author Contributions: Conceptualization, A.K. and P.M.; methodology, A.K. and P.M.; numerical experiments, A.K.; LGM experiment with INM-CM-4.8, P.M.; analysis, A.K. and P.M.; writing, A.K. and P.M. All authors have read and agreed to the published version of the manuscript.

Funding: This research was funded by the Russian Science Foundation (project 19-17-00215—calculations of runoff changes using hydrological model), the Governmental Order to Water Problems Institute, Russian Academy of Sciences (subject no. FMWZ-2022-0001—calculations of runoff changes by GCMs), the Governmental Order to Institute of Geography, Russian Academy of Sciences (subject no. FMGE-2019-0009—calculations of climate change and PMIP4-CMIP6 experiments with INM-CM-4.8).

Institutional Review Board Statement: Not applicable.

Informed Consent Statement: Not applicable.

Data Availability Statement: The GCM output data are available on the website (data link https://esgf-node.llnl.gov/search/cmip6/, accessed on 31 December 2022).

Acknowledgments: The authors are grateful to PMIP4 for the GCM output data. P.M. thanks Evgeny Volodin and INM RAS for help with the INM-CM simulation.

Conflicts of Interest: The authors declare no conflict of interest.

References

1. Rychagov, G.I. *Pleistocene History of the Caspian Sea*; Publishing House of the Moscow University: Moscow, Russia, 1997.
2. Yanina, T.; Sorokin, V.; Bezrodnykh, Y.; Romanyuk, B. Late Pleistocene Climatic Events Reflected in the Caspian Sea Geological History (Based on Drilling Data). *Quat. Int.* **2018**, *465*, 130–141. [CrossRef]
3. Yanina, T.A. Correlation of the Late Pleistocene Paleogeographical Events of the Caspian Sea and Russian Plain. *Quat. Int.* **2012**, *271*, 120–129. [CrossRef]
4. Tudryn, A.; Chalié, F.; Lavrushin, Y.A.; Antipov, M.P.; Spiridonova, E.A.; Lavrushin, V.; Tucholka, P.; Leroy, S.A.G. Late Quaternary Caspian Sea Environment: Late Khazarian and Early Khvalynian Transgressions from the Lower Reaches of the Volga River. *Quat. Int.* **2013**, *292*, 193–204. [CrossRef]
5. Bolikhovskaya, N.S.; Makshaev, R.R. The Early Khvalynian Stage in the Caspian Sea Evolution: Pollen Records, Palynofloras and Reconstructions of Paleoenvironments. *Quat. Int.* **2020**, *540*, 10–21. [CrossRef]
6. Kurbanov, R.; Murray, A.; Thompson, W.; Svistunov, M.; Taratunina, N.; Yanina, T. First Reliable Chronology for the Early Khvalynian Caspian Sea Transgression in the Lower Volga River Valley. *Boreas* **2021**, *50*, 134–146. [CrossRef]
7. Krijgsman, W.; Tesakov, A.; Yanina, T.; Lazarev, S.; Danukalova, G.; Van Baak, C.G.C.; Agustí, J.; Alçiçek, M.C.; Aliyeva, E.; Bista, D.; et al. Quaternary Time Scales for the Pontocaspian Domain: Interbasinal Connectivity and Faunal Evolution. *Earth-Sci. Rev.* **2019**, *188*, 1–40. [CrossRef]
8. Yanina, T.A. Environmental Variability Of The Ponto-Caspian And Mediterranean Basins During The Last Climatic Macrocycle. *Geogr. Environ. Sustain.* **2020**, *13*, 6–23. [CrossRef]
9. Kislov, A.; Toropov, P. East European River Runoff and Black Sea and Caspian Sea Level Changes as Simulated within the Paleoclimate Modeling Intercomparison Project. *Quat. Int.* **2007**, *167–168*, 40–48. [CrossRef]
10. Eyring, V.; Bony, S.; Meehl, G.A.; Senior, C.A.; Stevens, B.; Stouffer, R.J.; Taylor, K.E. Overview of the Coupled Model Intercomparison Project Phase 6 (CMIP6) Experimental Design and Organization. *Geosci. Model Dev.* **2016**, *9*, 1937–1958. [CrossRef]
11. Morozova, P.A.; Ushakov, K.V.; Semenov, V.A.; Volodin, E.M. Water budget of the Caspian sea in the Last Glacial Maximum by data of experiments with mathematical models. *Water Resour.* **2021**, *48*, 823–830. [CrossRef]
12. Hughes, A.L.C.; Gyllencreutz, R.; Lohne, Ø.S.; Mangerud, J.; Svendsen, J.I. The Last Eurasian Ice Sheets—A Chronological Database and Time-slice Reconstruction, DATED-1. *Boreas* **2016**, *45*, 1–45. [CrossRef]
13. Panin, A.V.; Sidorchuk, A.Y.; Ukraintsev, V.Y. The Contribution of Glacial Melt Water to Annual Runoff of River Volga in the Last Glacial Epoch. *Water Resour.* **2021**, *48*, 877–885. [CrossRef]
14. Utkina, A.O.; Panin, A.V. Upper Volga's Incision Valleys: Geomophological Aspects and Development History. *Geomorphology* **2022**, *53*, 162–172. [CrossRef]
15. Gosling, S.N.; Arnell, N.W. Simulating Current Global River Runoff with a Global Hydrological Model: Model Revisions, Validation, and Sensitivity Analysis. *Hydrol. Process.* **2011**, *25*, 1129–1145. [CrossRef]
16. Müller Schmied, H.; Eisner, S.; Franz, D.; Wattenbach, M.; Portmann, F.T.; Flörke, M.; Döll, P. Sensitivity of Simulated Global-Scale Freshwater Fluxes and Storages to Input Data, Hydrological Model Structure, Human Water Use and Calibration. *Hydrol. Earth Syst. Sci.* **2014**, *18*, 3511–3538. [CrossRef]
17. Haddeland, I.; Heinke, J.; Voß, F.; Eisner, S.; Chen, C.; Hagemann, S.; Ludwig, F. Effects of Climate Model Radiation, Humidity and Wind Estimates on Hydrological Simulations. *Hydrol. Earth Syst. Sci.* **2012**, *16*, 305–318. [CrossRef]
18. Veldkamp, T.I.E.; Zhao, F.; Ward, P.J.; de Moel, H.; Aerts, J.C.J.H.; Schmied, H.M.; Portmann, F.T.; Masaki, Y.; Pokhrel, Y.; Liu, X.; et al. Human Impact Parameterizations in Global Hydrological Models Improve Estimates of Monthly Discharges and Hydrological Extremes: A Multi-Model Validation Study. *Environ. Res. Lett.* **2018**, *13*, 055008. [CrossRef]
19. Krysanova, V.; Donnelly, C.; Gelfan, A.; Gerten, D.; Arheimer, B.; Hattermann, F.; Kundzewicz, Z. How the Performance of Hydrological Models Relates to Credibility of Projections under Climate Change. *Hydrol. Sci. J.* **2018**, *63*, 696–720. [CrossRef]
20. Shiklomanov, I.; Georgievskii, V.; Babkin, V.; Balonishnikova, Z. Research Problems of Formation and Estimation of Water Resources and Water Availability Changes of the Russian Federation. *Russ. Meteorol. Hydrol.* **2010**, *35*, 13–19. [CrossRef]
21. Georgiadi, A.; Miluykova, I. Possible Scales of Hydrological Changes in the Volga Basin under Anthropogenic Climate Warming. *Russ. Meteorol. Hydrol.* **2002**, *2*, 54–59.
22. Peel, M.; Blöschl, G. Hydrological Modeling in a Changing World. *Prog. Phys. Geogr. Earth Environ.* **2011**, *35*, 249–261. [CrossRef]
23. Krysanova, V.; Hattermann, F.; Kundzewicz, Z. How Evaluation of Hydrological Models Influences Results of Climate Impact Assessment—an Editorial. *Clim. Change* **2020**, *163*, 1121–1141. [CrossRef]
24. Kalugin, A. Hydrological and Meteorological Variability in the Volga River Basin under Global Warming by 1.5 and 2 Degrees. *Climate* **2022**, *10*, 107. [CrossRef]
25. Krysanova, V.; Vetter, T.; Eisner, S.; Huang, S.; Pechlivanidis, I.; Strauch, M.; Gelfan, A.; Kumar, R.; Aich, V.; Arheimer, B.; et al. Intercomparison of Regional-Scale Hydrological Models and Climate Change Impacts Projected for 12 Large River Basins Worldwide-a Synthesis. *Environ. Res. Lett.* **2017**, *12*, 105002. [CrossRef]
26. Kageyama, M.; Albani, S.; Braconnot, P.; Harrison, S.P.; Hopcroft, P.O.; Ivanovic, R.F.; Lambert, F.; Marti, O.; Peltier, W.R.; Peterschmitt, J.-Y.; et al. The PMIP4 Contribution to CMIP6–Part 4: Scientific Objectives and Experimental Design of the

PMIP4-CMIP6 Last Glacial Maximum Experiments and PMIP4 Sensitivity Experiments. *Geosci. Model Dev.* **2017**, *10*, 4035–4055. [CrossRef]
27. Kageyama, M.; Harrison, S.P.; Kapsch, M.-L.; Lofverstrom, M.; Lora, J.M.; Mikolajewicz, U.; Sherriff-Tadano, S.; Vadsaria, T.; Abe-Ouchi, A.; Bouttes, N.; et al. The PMIP4 Last Glacial Maximum experiments: Preliminary results and comparison with the PMIP3 simulations. *Clim. Past* **2021**, *17*, 1065–1089. [CrossRef]
28. Peltier, W.R.; Argus, D.F.; Drummond, R. Space Geodesy Constrains Ice Age Terminal Deglaciation: The Global ICE-6G_C (VM5a) Model: Global Glacial Isostatic Adjustment. *J. Geophys. Res. Solid Earth* **2015**, *120*, 450–487. [CrossRef]
29. Sidorenko, D.; Rackow, T.; Jung, T.; Semmler, T.; Barbi, D.; Danilov, S.; Dethloff, K.; Dorn, W.; Fieg, K.; Goessling, H.F.; et al. Towards Multi-Resolution Global Climate Modeling with ECHAM6–FESOM. Part I: Model Formulation and Mean Climate. *Clim. Dyn.* **2015**, *44*, 757–780. [CrossRef]
30. Volodin, E.M.; Mortikov, E.V.; Kostrykin, S.V.; Galin, V.Y.; Lykossov, V.N.; Gritsun, A.S.; Diansky, N.A.; Gusev, A.V.; Iakovlev, N.G.; Shestakova, A.A.; et al. Simulation of the Modern Climate Using the INM-CM48 Climate Model. *Russ. J. Numer. Anal. Math. Model.* **2018**, *33*, 367–374. [CrossRef]
31. Hajima, T.; Watanabe, M.; Yamamoto, A.; Tatebe, H.; Noguchi, M.A.; Abe, M.; Ohgaito, R.; Ito, A.; Yamazaki, D.; Okajima, H.; et al. Development of the MIROC-ES2L Earth System Model and the Evaluation of Biogeochemical Processes and Feedbacks. *Geosci. Model Dev.* **2020**, *13*, 2197–2244. [CrossRef]
32. Mauritsen, T.; Bader, J.; Becker, T.; Behrens, J.; Bittner, M.; Brokopf, R.; Brovkin, V.; Claussen, M.; Crueger, T.; Esch, M.; et al. Developments in the MPI-M Earth System Model Version 1.2 (MPI-ESM1.2) and Its Response to Increasing CO_2. *J. Adv. Model. Earth Syst.* **2019**, *11*, 998–1038. [CrossRef]
33. Motovilov, Y.G.; Gottschalk, L.; Engeland, K.; Rodhe, A. Validation of a Distributed Hydrological Model against Spatial Observations. *Agricult. For. Meteorol.* **1999**, *98–99*, 257–277. [CrossRef]
34. Motovilov, Y.; Danilov-Danilyan, V.; Dod, E.; Kalugin, A. Assessing the Flood Control Effect of the Existing and Projected Reservoirs in the Middle Amur Basin Based on Physical-Mathematical Hydrological Models. *Water Resour.* **2015**, *42*, 580–593. [CrossRef]
35. Bugaets, A.; Gartsman, B.; Gelfan, A.; Motovilov, Y.; Sokolov, O.; Gonchukov, L.; Kalugin, A.; Moreido, V.; Suchilina, Z.; Fingert, E. The Integrated System of Hydrological Forecasting in the Ussuri River Basin Based on the ECOMAG Model. *Geosciences* **2018**, *8*, 5. [CrossRef]
36. Kalugin, A. The Impact of Climate Change on Surface, Subsurface and Groundwater Flow: A Case Study of the Oka River (European Russia). *Water Resour.* **2019**, *46*, S31–S39. [CrossRef]
37. Gelfan, A.; Kalugin, A.; Krylenko, I.; Nasonova, O.; Gusev, Y.; Kovalev, E. Does a Successful Comprehensive Evaluation Increase Confidence in a Hydrological Model Intended for Climate Impact Assessment? *Clim. Change* **2020**, *163*, 1165–1185. [CrossRef]
38. Kalugin, A.; Lebedeva, L. Runoff Generation at the Small Permafrost River Basin in Eastern Siberia: Data Analysis and Hydrological Modeling. *E3S Web Conf.* **2020**, *163*, 01006. [CrossRef]
39. Kalugin, A. Process-Based Modeling of the High Flow of a Semi-Mountain River under Current and Future Climatic Conditions: A Case Study of the Iya River (Eastern Siberia). *Water* **2021**, *13*, 1042. [CrossRef]
40. Kalugin, A. Future Climate-Driven Runoff Change in the Large River Basins in Eastern Siberia and the Far East Using Process-Based Hydrological Models. *Water* **2022**, *14*, 609. [CrossRef]
41. Kalugin, A. Climate Change Attribution in the Lena and Selenga River Runoff: An Evaluation Based on the Earth System and Regional Hydrological Models. *Water* **2022**, *14*, 118. [CrossRef]
42. Motovilov, Y. Hydrological Simulation of River Basins at Different Spatial Scales: 1. Generalization and Averaging Algorithms. *Water Resour.* **2016**, *43*, 429–437. [CrossRef]
43. Gelfan, A.; Kalugin, A.; Motovilov, Y. Assessing Amur Water Regime Variations in the XXI Century with Two Methods Used to Specify Climate Projections in River Runoff Formation Model. *Water Resour.* **2018**, *45*, 307–317. [CrossRef]
44. Smith, M.W.; Riseborough, D.W. Climate and the Limits of Permafrost: A Zonal Analysis. *Permafr. Periglac. Process* **2002**, *13*, 1–15. [CrossRef]
45. Velichko, A.A. *Paleoclimates and Paleoenvironments of Extra-Tropical Regions of the Nothern Hemisphere. Late Pleistocene–Holocene. Atlas-Monograph*; GEOS: Moscow, Russia, 2009.
46. Borisiva, O.K. Landscape and Climatic Conditions in the Central East European Plain in the Last 22 Thousand Years: Reconstruction Based on Paleobotanical Data. *Water Resour.* **2021**, *48*, 886–896. [CrossRef]
47. Gelfan, A.; Kalugin, A. Permafrost in the Caspian Basin as a Possible Trigger of the Late Khvalynian Transgression: Testing Hypothesis Using a Hydrological Model. *Water Resour.* **2021**, *48*, 831–843. [CrossRef]
48. Kislov, A.V.; Morozova, P.A. Level Variations in the Caspian Sea under Different Climate Conditions by the Data of Simulation under CMIP6 Project. *Water Resour.* **2021**, *48*, 844–853. [CrossRef]
49. Svitoch, A.A. The regime of the Caspian Sea level reconstructed using paleographic data. *Water Resour.* **1997**, *24*, 9–18.